Science of Remote Sensing 12 (2025) 100246

Contents lists available at ScienceDirect

Science of Remote Sensing

journal homepage: www.sciencedirect.com/journal/science-of-remote-sensing

A comparative study of voxel-based leaf area density estimation from quantitative structure models of trees

Qiguan Shu [a,*], Thomas Rötzer [b], Hadi Yazdi [a], Astrid Reischl [b], Ferdinand Ludwig [a]

[a] Professorship for Green Technologies in Landscape Architecture, TUM School of Engineering and Design, Technical University of Munich, Germany
[b] Chair for Strategic Landscape Planning and Management, Technical University of Munich, Germany

ARTICLE INFO

Keywords:
Urban forestry
Terrestrial laser scanning
Quantitative structural model
Leaf area density
Tree information modeling

ABSTRACT

This study explores the potential of using Quantitative Structure Models (QSM) to predict trees' voxel-based Leaf Area Density (LAD) to reduce the workload and data redundancy in studying deciduous trees. For this purpose, leaf-on and leaf-off Terrestrial Laser Scanning (TLS) of 16 *Platanus x hispanica* trees on streets were utilized. QSMs were extracted and interpreted into QSM indexes corresponding to voxels, a novel approach introduced in this study. Twelve standard regression models were tested to predict the LAD value for each voxel using its QSM indexes. The Hist Gradient Boosting Regressor (HGBR) model demonstrated the best performance, with an R-squared score of 0.56 and a mean absolute error of 0.0187 m^2/m^3 (16.33 %) in the LAD prediction. This deviation mainly happened at the crown center, where branches were dense while leaves were few. The trained model was also applied to another set of 13 young plane trees of different tree sizes at a nursery. Their predicted Leaf Area Index (LAI) was compared to the LAI measured indirectly by hemispherical photography, showing a deviation of 0.12 m^2/m^2 (8.6 %) for the 3 largest trees with the closest Diameter at Breast Height (DBH) to the street trees. The deviations are larger for young nursery trees with smaller DBHs. Therefore, further experiments are needed to optimize the voxel size and adapt the model to different species with varying crown sizes.

1. Introduction

Terrestrial laser scanning (TLS) has been widely applied in forestry studies for over two decades due to its high efficiency and accuracy in surveying tree stands in detail (Akay et al., 2009; Ralph and Jason, 2000). In the past ten years, both hardware devices (Kükenbrink et al., 2022) and algorithms have evolved to capture individual trees with dense point clouds (Åkerblom and Kaitaniemi, 2021; Calders et al., 2020; Döllner et al., 2023). In recent years, workflows have been published to facilitate this digital procedure, such as TLS2trees (Wilkes et al., 2023) for tree segmentation. Further methods to extract specific tree indexes from segmented point clouds can vary depending on research purposes. For example, the ITSMe package in R language (Terryn et al., 2022) identifies a tree's crown and trunk and measures its height, diameter at breast height (DBH), crown projection area, etc. AdTree (Du et al., 2019) and treeQSM (Raumonen, 2022; Raumonen et al., 2013) build cylindrical models of tree branches, which can be used for estimating woody biomass. These show an irreversible trend that forestry and tree-survey-related studies rely more on accurate quantitative data about trees than ever before. Meanwhile, related researchers have more efficient tools with easier access.

When investigating deciduous trees, their leaf areas fluctuate periodically following seasonal environmental conditions. Consequently, performing leaf-on scans in summer and leaf-off scans in winter (or early spring) has different utilities. In leaf-on scans, the laser beam is transmitted through overlapped leaves and returns with multiple echoes at different distances and intensities (Grau et al., 2017). Although not every single leaf is captured, the data is used to study leaf angle (Stovall et al., 2021), leaf area, and density (Wei et al., 2020). However, the occlusions are hardly compensated by refining the rotational angular resolution and shortening distances between scanning positions (Abegg et al., 2017). Especially for surveying forest inventory, the occlusions in leaf-on scans become so intensive that TLS is complemented by new lightweight sensors on uncrewed aerial vehicles (Schneider et al., 2019). Therefore, when the leaves are not the studying objects but DBH, tree height, woody branches, and sometimes objects behind or in the tree crowns, leaf-off scans are a proper and more efficient choice on deciduous trees.

Over the last decade, the leaf-on and leaf-off scans have been adapted for the study of urban green systems (UGS). Deciduous species are the

* Corresponding author.
E-mail address: qiguan.shu@tum.de (Q. Shu).

https://doi.org/10.1016/j.srs.2025.100246
Received 15 May 2025; Received in revised form 3 June 2025; Accepted 4 June 2025
Available online 6 June 2025

most common woody plants in European cities (Alós Ortí et al., 2022; Weller, 2021). They provide essential ecosystem services (ESS), such as cooling and shading against the urban heat island (UHI) effects (Parsa et al., 2019; Rahman et al., 2020). Urban trees, especially deciduous trees, improve climate adaptation in cities. Next to their climate regulating services (Reid et al., 2005), they offer ESS like reduction of run-off (Armson et al., 2013; Rahman et al., 2022), carbon storage and sequestration (Strohbach and Haase, 2012), habitat provision (Kowarik et al., 2020), air purification (Kroeger et al., 2018; Mcdonald et al., 2018), noise buffering, recreational benefits and an overall increase of property value due to their presence (Bolund & Hunhammar, 1999; Wolf et al., 2020). The ESS of urban trees is important for creating sustainable and resilient cities and enhancing the overall quality of urban life (Duinker et al., 2015).

Leaf-on scans facilitate an estimation of leaf area density (LAD) in voxel grids (Hosoi et al., 2013; Soma et al., 2021). It is linked to the evaluation of a tree's canopy performance such as shading or transpiration (Eyster and Beckage, 2023; Rahman et al., 2020). Leaf-off scans facilitate the collection of structural data of a tree such as DBH, tree height, and woody biomass. They are essential to represent the tree growth (i.e., used in the CityTree model (Rötzer et al., 2019)). Besides, leaf-off scans can also facilitate the management of urban trees in horticultural practice through quantitative structure tree models (QSM) (Shu et al., 2024). Based on these requirements, to design and plan UGS targeted towards multi-functional uses (Yazdi et al., 2023), both leaf-off and leaf-on scans are obligatory in completing the database that contains structural and functional components of urban trees (see also tree information modeling (Shu et al., 2022)). This would require two scans of the same scene and trees in the same year (at least one in summer, the other in winter or early spring).

In principle, the leaves are not randomly scattered within a crown space. Initiated from apical buds, their distribution pattern follows specific regulation of phyllotaxis (Krishnamurthy et al., 2015). Consequently, their number, total area, and distribution are strongly connected with the position and status of internodes and branches (see Fig. 1a). Such relations have been utilized in classical virtual plant models by an L-system (Prusinkiewicz and Lindenmayer, 1996), where leaves' position, size, and inclination angle are coded based on the internode structure of plants. With this feature, functional structural plant models (FSPMs) by L-system was used over 15 years ago to study how the leaf architecture affects branch growth through light absorption (Pearcy et al., 2005; Sarlikioti et al., 2011). In reverse, leaf distribution was simulated based on branching patterns (Prusinkiewicz et al., 2001). Those imitated leaves were used to estimate the leaf area (Hemmerling et al., 2008), LAD (Jin and Tamura, 2012), and Leaf Area Index (LAI) (Jonckheere et al., 2006) of the virtual tree.

Inspired by these studies, this paper addresses the following research question: Does a correlation exist between the spatial distribution of woody branches and leaf area distribution in real-world applications? The real-world applications emphasized in this study are constrained by current technical limitations and data precision. Regarding the woody structures, we observed that TLS could not capture every detailed twig that connects to individual leaves in the leaf-off state of a tree (see missing details in Fig. 1b). Although recently developed QSMs contain topological and geometrical information in describing branch structures (Raumonen et al., 2013; Shu et al., 2022), many other features (i.e. barks and nodes) are overlooked. Therefore, the objective of this study is to ascertain whether voxel-based LAD for real trees, as extracted from leaf-on scans (see Fig. 1c), can also be estimated from specific woody branch distribution indexes acquired in leaf-off scans (see Fig. 1b).

Answering this question has significant implications: 1) the leaf-on scan of urban trees can be omitted to estimate voxel-based LAD; 2) gardeners of the future, when manipulating branches in the leaf-off stage of a tree, could also get feedback on the effects on the leaves. For these two reasons, this study is a foundation for how the future UGS will be designed and managed (Ludwig et al., 2024; Yazdi et al., 2023).

2. Method

2.1. Data collection by TLS

The dataset for studying the QSM-LAD relation requires TLS of trees with both their leaf-off scans to extract the QSM of the trees and leaf-on scans to estimate their LAD. The trees with leaf-off scans are retrieved from the open-sourced multilayered urban tree dataset named TreeML-Data (Yazdi et al., 2024). It contains the TLS and QSM of street trees collected in Munich in January of 2023 at 40 different streets scattered around the city using the scanner Riegl VZ-400i. In this case, the scanner was mounted on a vehicle, which stopped at each scanning position. For the study at hand, 16 Platanus *x hispanica* from this database in one street were used (see Fig. 2a). They were manually segmented out to individual point clouds (see Fig. 2b; locations and detailed measurements can be found in the Supplementary Table 1). Considerations for selecting them were: 1) these were tall plane trees with DBH larger than 30 cm so that they could grow a dense canopy; 2) they were planted along one single street, enabling efficient scans for having their leaf-on status; 3) plane trees are one of the most common urban trees in European cities. Besides, the LAD estimation for *P. x hispanica* can be applied to other data of the same species in previous projects conducted by the authors (see section 2.5).

Based on these leaf-off scans, the selected 16 plane trees were scanned by the authors again with their leaves-on at the end of July 2023 (see Fig. 2e) for this study. The scanner, settings, and processing method were identical to the previous leaf-off scans. The point clouds from individual scans were registered with RiSCAN Pro. The registration is in reference to the GPS coordinates of the scanning position recorded

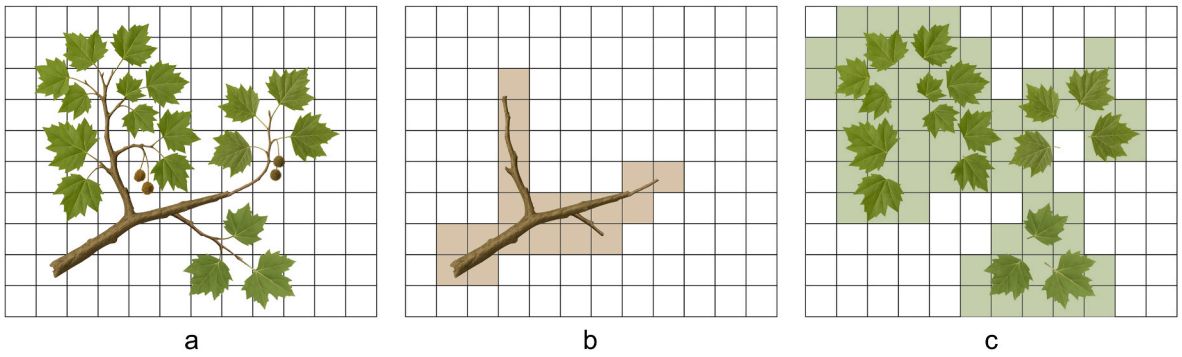

Fig. 1. The concept of associating the distribution of detectable branch structures in leaf-off scans with the distribution of leaves in leaf-on scans. a): a plane tree branch overlaid on plane grids as an example; b) occupancy of major woody structures that can be captured by TLS at its leaf-off state; c) the aim of predicting leaf distribution in the grids from the detectable woody structure.

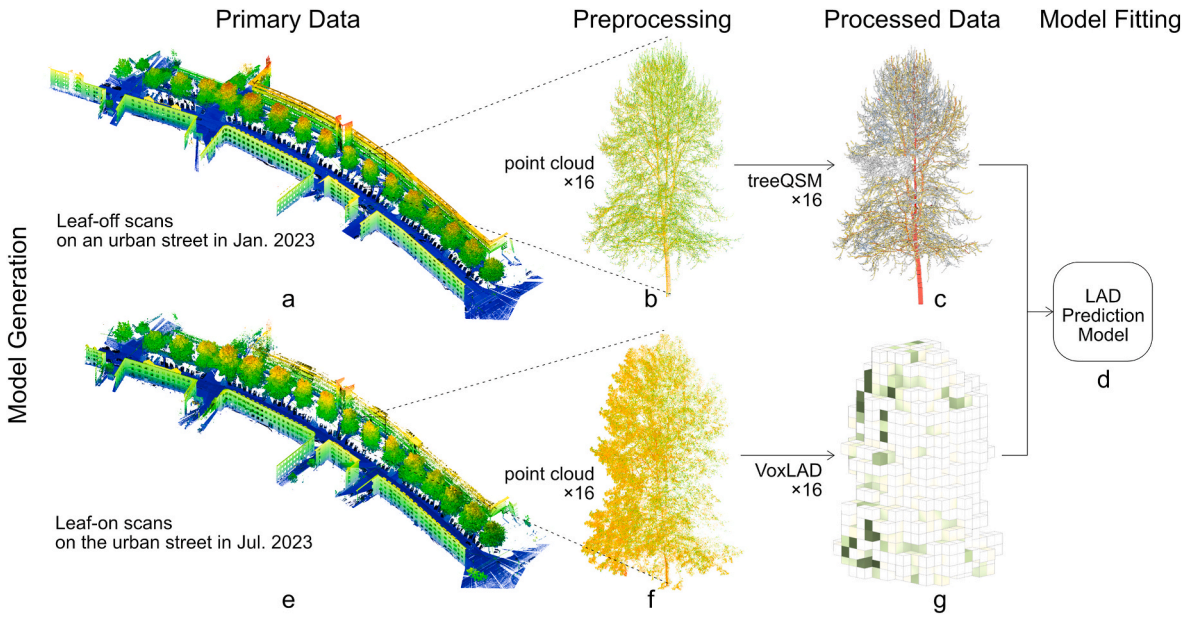

Fig. 2. An overview of the data source and the process to generate the voxel-based LAD prediction model using QSM. a) and e): Leaf-on and leaf-off scans of the same street in Munich using Riegl TLS. b) and f): Segmented point clouds for individual trees. c) QSM of trees using treeQSM on the leaf-off scans. g) LAD in voxels using VoxLAD on the leaf-on scans. d) Testing performances of different models.

by Leica Zeno FLX100 with an accuracy of ca. 2 cm (Yazdi et al., 2024). In this approach, the point clouds of leaf-off and leaf-on scans are perfectly aligned in the global coordinate system (Wu, 2021). With a visual check of the overlapped leaf-on scans on the leaf-off scans, no mismatching is detected on stiff surfaces such as the pavement, building facades, and thick woody trunks. Afterward, the 16 individual trees were roughly cut out from the scene through a cloud-to-cloud distance filter in reference to the segmented trees in leaf-off scans using Cloudcompare (Girardeau-Montaut, 2023). The fine segmentation was adjusted on this base manually (see Fig. 2f).

2.2. Reconstruction of quantitative structural models (QSMs)

The point clouds of individual trees from leaf-off scans (see an example in Fig. 2b) were used for generating QSMs. QSM is a cylindrical representation of tree trunks and branches. It contains the tree's typological structure, such as the parent and children of each cylinder and its hierarchy order among all tree branches. Many open-source tools are developed for reconstructing the QSM out of a point cloud include PypeTree (Delagrange et al., 2014), SimpleTree (Hackenberg et al., 2015), 3D forest (Trochta et al., 2017), treeQSM (Raumonen, 2022; Raumonen et al., 2013), Adtree (Du et al., 2019) and AdQSM (Fan et al., 2020). Through primary testing of these tools on the collected data, it is noted that PypeTree, Adtree, and AdQSM have a high requirement for clarity of the point cloud. They use Dijkstra's shortest path to create skeletons from the points at the crown top to the trunk base. Once the noise in the crown becomes slightly intense, this approach will "invent" fake twigs. SimpleTree embeds an outdated Qt library version, making it incompatible with later-developed methods. Therefore, treeQSM was chosen for QSM reconstruction. It breaks down the point cloud of a tree into patches of points following the Voronoi partition. Then, it fits the cylinders to those patches using the least square, and thus, it is a robust method on our dataset to describe the branching structure despite the uncleared noises.

The two parameters that decide the patch sizes are the most important settings in altering the quality of cylinder fitting in treeQSM, namely the minimum and maximum patch diameters. The smaller patch can capture more details in the twigs but is getting more sensitive to the gaps within the same branches due to occlusion. In our implementation, considering various twig sizes for urban trees, we require the minimum patch diameter to be calculated at 0.01, 0.02, and 0.03 m. Accordingly, the maximum patch diameter was required using 0.07 and 0.10 m due to thin or thick stems. The decisions of these settings follow the instructions in treeQSM's manual book (Raumonen, 2022): firstly, the size of these patches should vary to balance the accuracy, memory consumption, and modeling time. More importantly, the branch segmentation is performed based on the connectivity of these patches. The bifurcations are identified as places where neighboring patches first disconnect. Afterward, the program fits cylinders to branches using the least squares fitting with a minimum surface coverage of 70 % for the stem and 40 % for the rest of the branches. QSMs will be generated using combinations of the required patch diameters for every tree to acquire the best-fitting result. Moreover, the random seeds for generating the patches impact the final performances. Therefore, the QSM reconstruction was also repeated 15 times for each patch diameter configuration on every tree to enhance their robustness against the impacts of pseudo-random numbers. Only the QSM with the minimum average point-cylinder distance is selected as the final QSM. For such a heavy computational load, the program was run on a virtual machine equipped with Intel(R) Xeon (R) Gold 6148 CPU @ 2.40 GHz and 45 GB RAM parallelly in 10 VCPU cores. Following this approach, 16 QSMs were obtained representing the 16 plane trees (see Fig. 2c).

2.3. Estimation of leaf area density

The point clouds of individual trees from leaf-on scans (see Fig. 2f) are used for estimating their leaf area density distributions (see Fig. 2g). To this purpose, several new methods have been developed in recent years using light transmittance (Mkaouar et al., 2019, 2021) and path length of the beam (Hu et al., 2018). However, the model VoxLAD (Béland et al., 2014), which uses straightforward ray tracing techniques, was implemented in this study because it has already been widely applied in various related studies (Dissegna et al., 2019; D. Wu et al., 2018; Yin et al., 2022). Therefore, its performance has been checked using multiple data sources and scenes. The main principle of VoxLAD is the contact frequency of the LiDAR beam with foliage in a given voxel, taking into account the inclination angles of both the beam and the leaf surface concerning the voxel's orientation (Béland et al., 2011). As a

result, voxel size (Soma et al., 2018), leaf inclination angle distribution (Jiang et al., 2021), and precise segmentation between points of foliage and points of the woody elements are the most critical settings to achieve reliable LAD estimations on TLS data.

2.3.1. Settings in VoxLAD

For the decision of the appropriate voxel size, it is shown in a previous study that the overall accuracy is strongly reduced with the increase of the voxel size after 0.3 m (Wei et al., 2020). However, it should be noted that this deviation is also closely related to LAD itself. In the tests by Wei et al., the deviation of the LAD at voxel sizes of 0.5 m and 1 m only becomes intensive for extremely dense foliage, where the LAD is higher than 3 m^2/m^3. LAD of common urban tree species' leaf area density is mostly less than 0.5 m^2/m^3 (in reference to Asef et al. (2020)). Therefore, the deviation with a voxel size in the range between 0.5 and 1.0 m is considered insignificant in our case. Soma et al. (2021) recommended a 0.5m voxel size to balance the accuracy and correction opportunities. In our next step to extract QSM indexes related to the voxels (see section 2.4), the voxel size should not be too small (compared to an average cylinder length) to cause a bias in the allocation process. Based on these considerations, the voxel size was set to 0.8 m in our study, serving as a primary test. One advantage of this size is its flexibility in aligning perfectly to smaller voxels of 0.1, 0.2, and 0.4 m lengths using an octree. The influence of voxel size in the LAD prediction must be addressed in future studies (for a discussion, see section 4.3).

The inclination angle of a leaf describes the angle between the leaf surface normal and the zenith (Raabe et al., 2015). For the tree to acquire more exposure to the sunlight, it was observed that the inclination angle of leaves is not identical throughout the tree crown but follows species-specific distribution patterns (Wit, 1965). These patterns were further summarized into six theoretical categories: erectophile, extremophile, plagiophile, planophile, spherical, and uniform (see i.e., Liu et al. (2019)). These categories were also taken as preset options in VoxLAD. Chianucci et al. (2018) measured leaf inclination angles for 138 deciduous broadleaf tree species, including 101 *P. x hispanica*. Their measurements confirmed that the plane trees' canopy should follow the plagiophile shape (see Fig. 3 left).

Besides the most critical settings in calculating LAD for each voxel by VoxLAD, there are some details to enhance the accuracy. First, the Rigel V-400i could capture numerous echoes of the pulses through the canopy. However, we kept only the first return in the point clouds for an accurate leaf area density calculation. Second, the points captured by different scanning positions were separated using an attribute named GPS time. It described the precise time when the points were captured. Our leaf-on scans took approx. 45 s each without interruption. The subsequent scan commenced at a minimum of one to 2 min after the initial procedure due to the relocation of the vehicle and the subsequent examination of the configurations. This allows the separation of captured points by different scanning positions to be very precise. Third, for calibrating the contact frequency errors, we also entered the ratio of the long axis by the short axis of a typical plane tree leaf as one and an average area of 314.16 cm^2 per leaf into VoxLAD. These parameters were directly measured from a few clearly shown leaf samples in the point clouds. Next, the angle resolution was set to 0.03°, the same as the scanner setting during the scanning. Lastly, VoxLAD outputs the estimated LAD from each scanning position separately. When the voxel was not visible from a scanning position, the LAD estimation was returned with zero. We took the average LAD values larger than zero from different scanning positions. This would further reduce the disturbances by the contact frequency error.

2.3.2. Point cloud segmentation for leaf and wood

In forestry studies, the segmentation between foliage and woody parts is mostly accomplished using trained machine-learning models (Krishna Moorthy et al., 2020), such as the open-source FSCT model (Krisanski et al., 2021) or TLS2trees (Wilkes et al., 2023). The limitations of these approaches are their robustness and adaptation to data that differs in its qualities or structures from the training dataset. Especially when our dataset deals with urban trees whose crown's starting heights are lower and whose crown diameters are larger than those trees in dense forests. Therefore, the points lower than a typical forest tree's height or those far from the trunk were mistakenly segmented into non-leaves with the trained FSCT model from Krisanski et al. (2021) (see Fig. 4 left). This will cause an overlook when calculating the LAD in these areas. To acquire a more precise result in segmenting the leaf and wood, we adopted an approach used by Kim et al. (2015) and Wang et al. (2018). They used the different intensities of foliage and woody surfaces to reflect laser beams to distinguish between them. The implementation of this approach is based on the Riegl V-Line LiDAR instruments, which record a so-called relative reflectivity (dB) value for each target echo. It is calibrated as the ratio of the actual optical amplitude versus the optical amplitude of a diffuse white target at the same range (Riegl, 2009). Derived from the equation given by Kim et al. (2015), we used equation (1) to transform the relative reflectance values into apparent reflectance (%) values. The separation between leaf and wood should be chosen at a threshold approximately midway of the highest values in the reflectance (Kim et al., 2015). For our tree sample (see Fig. 3 right), the maximum apparent reflectance value was approximately 0.7, and the threshold at half of it (0.35) was precisely where the number of returns in the leaf-on scans met the leaf-off scans on the same tree. This is why 0.35 was chosen to segment wood and leaf in this study. As the LAD calculation approach by Béland et al. (2011) required the exclusion of the pulses that only partially hit a leaf, this could be solved with apparent reflectance as well by another threshold of 50 % of the nominal (spectrometer-measured) leaf reflectance value (Kim et al., 2015). In our data sample, the peak of the leaf returning numbers had an apparent reflectance at around 0.2. Based on this, we chose 0.1 as the threshold to separate noise (where the pulses only partially hit leaves) and leaves (where pulses mostly hit leaves). This threshold was also at a turning point where the number of laser returns

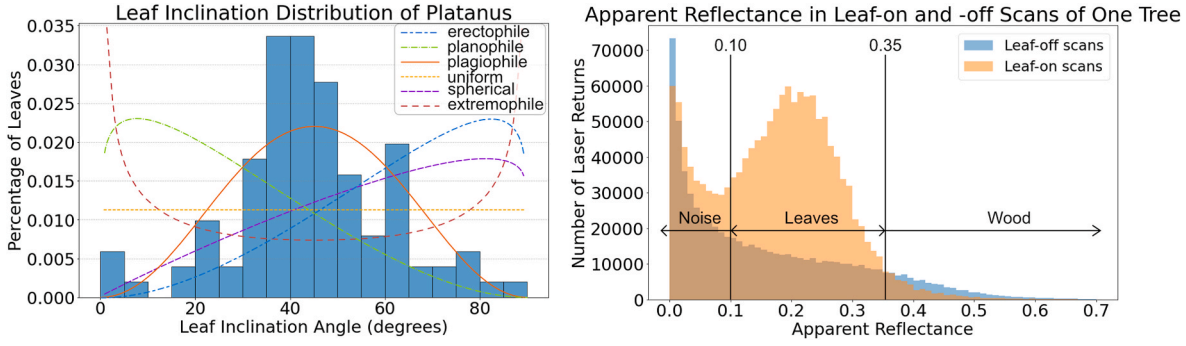

Fig. 3. Left: Leaf Inclination Angle Distribution of P. x hispanica (data from Chianucci et al. (2018) in blue bar graphs) compared to the six theoretic inclination distribution categories. Right: Point segmentation using a comparison between apparent reflectance distributions in Leaf-on and off scans of one tree.

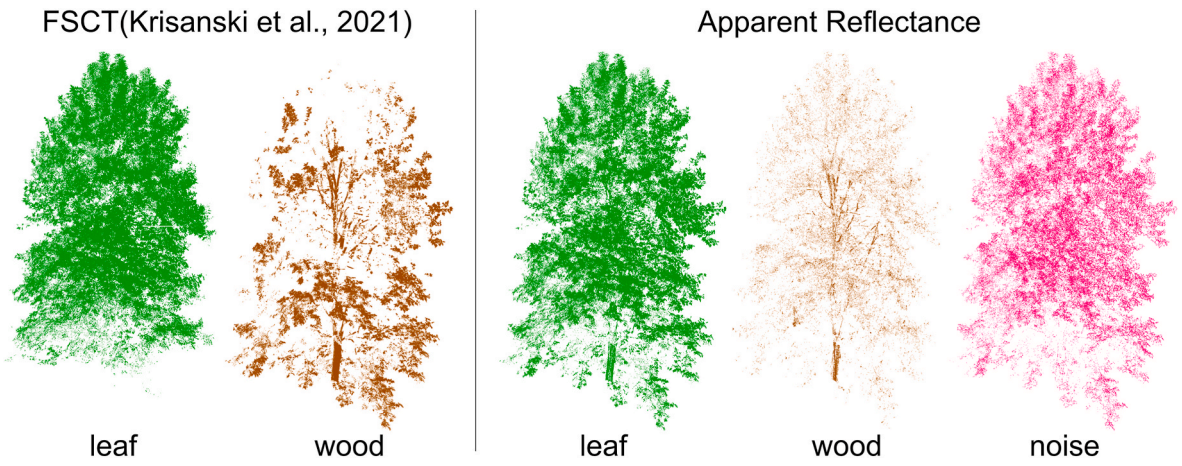

Fig. 4. Comparison of two segmentation effects on our dataset. Left: Segmentation of leaf and wood using FSCT (Krisanski et al., 2021). Right: segmentation of noise, leaf, and wood points using their apparent reflectance.

climbed as the apparent reflectance went further up (see Fig. 3 right). Using this method above, we acquired the precise labeled point clouds regarding leaf, wood, and noise (see Fig. 4 right) for predicting LAD with the approach by Béland et al. (2011).

$$Apparent\ Reflectance = 10^{-\left|\frac{Relative\ Reflectivity\ (dB)}{10}\right|} \quad (1)$$

2.3.3. Use of partial canopy data for estimation

Due to scanning limitations and potential occultation effects, only the street-facing half of each tree canopy was used for LAD estimation. The estimated LAD of one tree with a voxel size of 0.8 m is illustrated in Fig. 5. The complete dataset can be found in the supplementary data files. All the trees are on one side of the street, close to a building. This resulted in all eight scanning positions on the northeast side of the crown only (see Fig. 5a). As seen in Fig. 5b and c, the back side of the canopy was estimated to have a much lower LAD than the front side. We could not analyze if the causes of this result were 1) intensive occultation, 2) the fact that the canopy grew less dense facing the building façade, or 3) a mix of both factors. To ensure a better LAD prediction model, we took up only the data from voxels facing the street to later steps. These voxels were filtered by a line parallel to the street (at around 135° to the east direction) through the location of each tree stem. Only voxels whose center was on the line's northeast side were considered as validated LAD estimations (see selected voxels within the rectangular boxes of the dotted line in Fig. 5b and c). These validated voxels are less affected by occultations, like the scanning at the nursery used for performance evaluation (see section 3.3). In contrast, the voxels facing the building deviate significantly from nursery trees in light conditions, etc. The data's final formatting and VoxLAD execution were conducted in MATLAB R2023b (The MathWorks Inc, 2024).

2.4. Extraction of QSM indexes for regression models

Following the preceding steps, LAD is estimated for each voxel independently and is not yet associated with individual cylinders in the QSM. To merge this gap, a novel QSM Index system was created in our study to extract certain information contained in QSM to voxel-based attributes. The QSMs originated from leaf-off scans (see section 2.2). Specifically, we first assign each cylinder of a QSM to the voxel that contains most of the cylinder's length (see Fig. 6b). In the implementation, this was calculated using the two ends and the middle point of the cylinder as sample points. This cylinder was allocated to one voxel if more than two of these three points were inside this voxel.

Then, the same method was repeated to allocate cylinders to a boundary box larger than the voxel. This way, we could understand the branch distribution (especially their numbers and sizes) in a larger context. To achieve this, we defined two cubic boundaries: one box with 3 times the length of the voxel (2.4 m, see Fig. 6c); 2) the other box with 5 times the length of the voxel (4.0 m, see Fig. 6d). They are named 3-

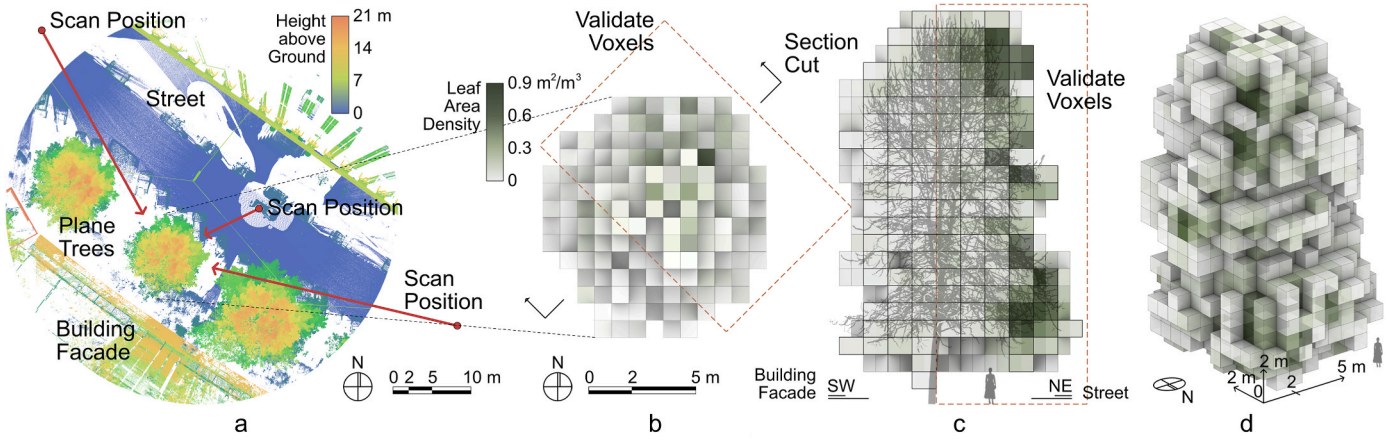

Fig. 5. Illustration of the LAD estimation by VoxLAD (Béland et al., 2011). a) A zoom-in section of the point cloud, where scan positions are only one-sided to trees while the building façade is on the other side. b) LAD voxels in the master plan view. c) LAD voxels in a section perpendicular to the street. The numbers are larger on the street side. d) The LAD voxels in 3D.

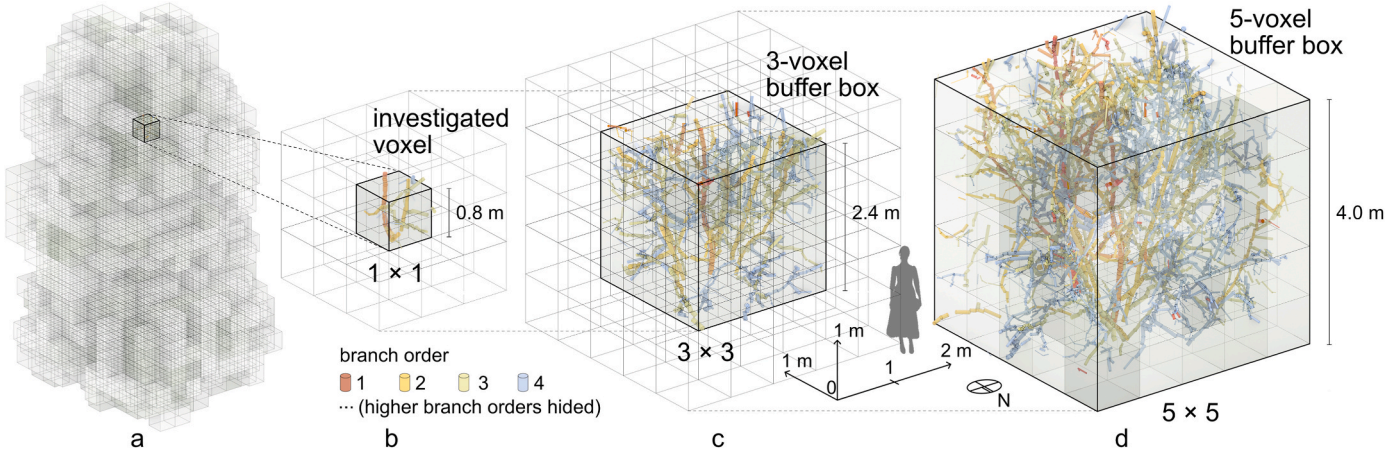

Fig. 6. An example of allocating cylinders to voxels. a) All voxels of one tree. b) Take one voxel as an example. It contains a few branches within the cube of 0.8 m in length for each side. c) Its 3-voxel buffer box is 2.4 m long for each side. d) Its 5-voxel buffer box is a cube with a side length of 4.0 m.

voxel buffer box and 5-voxel buffer box respectively in the following texts. These two buffer boxes captured cylinders in close- and far-range surroundings. As the leaves are expected to be denser at the outer side of the crown than the crown center (see Fig. 5c), the assumption is that the statistics of cylinder distributions in the surroundings, especially the 5-voxel buffer box, can better reflect the relative position of this voxel to the overall crown. The necessity of the two buffer boxes is discussed in section 4.3.

For each voxel of a tree, we extracted 138 indexes named QSM index to describe features of the cylinder distribution within the voxel itself and its 3- and 5-voxel buffer boxes. These indexes were features of the cylinders' number, length, radius, volume, and direction. These indexes also described their branch order, position in their branch, distance, and relative pitch direction from the voxel center. The complete list of these QSM indexes is explained in Supplementary Table 2. Pearson correlations of these indexes on our dataset are illustrated in Supplementary Fig. 1. The raw data is available in the supplementary data files.

The 16 trees consist of 76 560 voxels in total. Each voxel has 138 QSM indexes used as the features, and its estimated LAD was the target. The whole dataset was randomly split into a training set and a testing set with a testing rate 0.2. We tested the performances of 12 standard regression models with sklearn in their default settings, including linear regression and support vector regression (Pedregosa et al., 2011) (see Supplementary Table 3). The model with the highest R-squared scores is selected as the final prediction model.

2.5. Application of the trained model

Given any leaf-off scans of a tree, a similar process can be followed to generate a voxel grid space in a defined boundary box and its QSM indexes for each voxel. In our study, this boundary box was always expanded 3 m in all six directions along the x, y, and z axis from the furthest outreach of the tree's branches. With QSM indexes of every voxel, its LAD value can be predicted using the trained regression models.

As a by-product, the LAI values in pixels on the floor plan are the sum of LAD values for voxels with the same x and y coordinates. The calculation is written in equation (2) (Rouzbeh Kargar et al., 2019), where h is the total height of the voxel space. Z is the coordinate in the z-axis of the voxel center. It helps visualize the LAD results in 2D grid

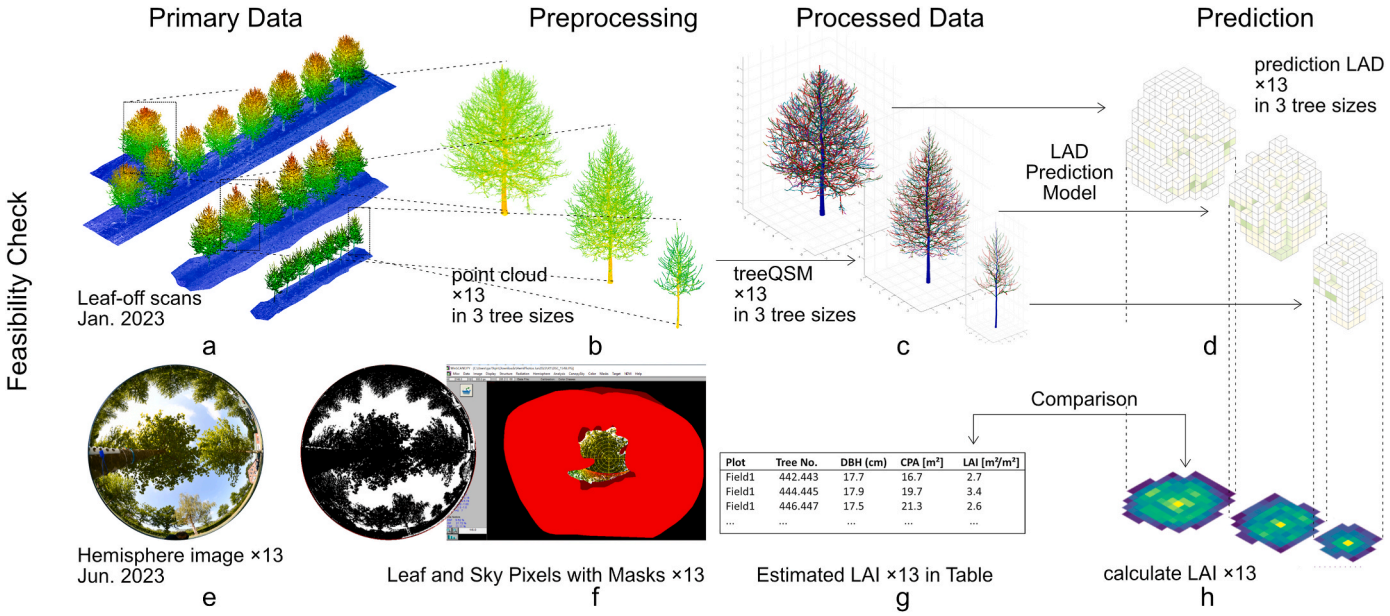

Fig. 7. The trained prediction model was applied to 13 younger plane trees in a nursery with 3 different sizes. Hemisphere Images were used to measure their LAI values in the summer.

maps (see Fig. 7h and Supplementary Figs. 3 and 4).

$$LAI = \sum_{z_i=0}^{h} LAD(z_i) \quad (2)$$

The trained model was further applied to predict LAD for other 13 *P. x hispanica* trees grown at Bruns Nursery close to Bremen (Northern Germany). These trees were grown in three fields (see Fig. 7a) and showed different ages, branch sizes, densities, etc. They were scanned with Riegl VZ-400i at the end of January 2023 in their leaf-off status. They were segmented manually and denoised with a SOR filter (Park et al., 2020) (see Fig. 7b). Their QSM indexes were extracted from QSMs to predict their LAD values in voxels (see Fig. 7c and d). The voxel size was kept the same (0.8 m) as the data used for the training prediction model.

To compare this LAI calculated from our prediction model with other methods, LAI measurement was conducted in June 2023 for a series of nursery trees with two hemisphere images beneath every tree crown (see Fig. 7e). A Nikon D7500 was used with a fisheye lens of brand Sigma. The fisheye lens enables pictures at 180° degrees so that the tree crowns are visible with their full extension in the picture. These hemisphere images were processed with the software WinSCANOPY Pro 2019a (Regens Instruments, Canada) based on the process of pixel classification (see Fig. 7f). We used the function "LAI2000Glog" for LAI calculation to differentiate sky and leaf area. Based on these, a single LAI value was calculated for each tree (see Fig. 7g and Supplementary Table 5).

3. Results

3.1. Model performances and the most important features in LAD prediction

The performance of a regression model can be evaluated with R-squared scores, mean absolute errors (MAE), and mean squared errors (MSE). The scores of the tested 12 models can be found in Supplementary Table 3. Among them, the Decision Tree Regressor, Support Vector Regression, and Ada Boost Regressor exhibited a negative R-squared value, showing a suboptimal performance for this task. In contrast, the performance indicators of the remaining 9 regression models are presented in Fig. 8 in ascending order of performance. The Hist Gradient Boosting Regressor (HGBR) offered the most accurate predictions with an R-squared score of 0.56. The MAE and MSE were 0.0187 (m^2/m^3) and 0.0029 respectively. Compared to average non-zero LAD values of 0.1145 m^2/m^3, the mean absolute error is around 16.33 %.

The HGBR model's most effective QSM index to predict the voxel-based LAD was the total cylinder number contained by the 3-voxel buffer box (see Fig. 9 left). It contributed around 50 % to the prediction accuracy according to its permutation importance. It is positively related to the predicted LAD, but a direct linear relation between these two factors is weak (see Fig. 9 right). The second most influential QSM index was followed by the average height difference from the voxel center to the cylinders' starting locations within the 3-voxel buffer box. Its contribution was around 20 %. In addition, the other three QSM Indexes contribute more than 10 % to the accuracy of the prediction (see Fig. 9 left). They are the average branch length in the 5-voxel buffer box, the total cylinder volume in the 3-voxel buffer box, and the maximum position sequence of the cylinders in their branches within the 5-voxel buffer box. In all QSM indexes, most of the effective features described the cylinder distribution within their surrounding buffered boxes (see index name in Fig. 9 left ending with "2" or "3"). Regarding the cylinders directly contained by the core voxel itself, only the average z direction from the voxel center to the starting locations made into top 10. It contributed around 2 % to the accuracy of the prediction.

3.2. Predicted LAD in voxels compared to the leaf-on scans

The spatial distribution of the LAD prediction was analyzed concerning height and distances to the trunk position (see Fig. 10).

The street trees in our dataset are unlike typical forest trees that compete intensively for light. Therefore, the captured plane trees do not grow dense crowns at the treetop. As the blue curves show, the highest density area in the canopy was around 4 m above the ground (see Fig. 10 left). This height was approximately 2 m higher than the crown's starts. LAD and leaf area decrease as the height increases up to the treetop. The predicted results also show these features (see the orange line). However, between the 3–15 m height, the predictions are slightly larger than the data from the training dataset.

Regarding the relation between LAD in voxels and their distances to the trunk (see Fig. 10 right), these scanned trees have an average crown radius of around 7 m. In the measured data by VoxLAD (see the blue line), the average LAD went below 0.02 m^2/m^3 beyond this distance to the trunk. Meanwhile, the LAD reached its peak of 0.08 m^2/m^3 at a 3.5-m distance (half of the crown radius) to the trunks. The overall trend of

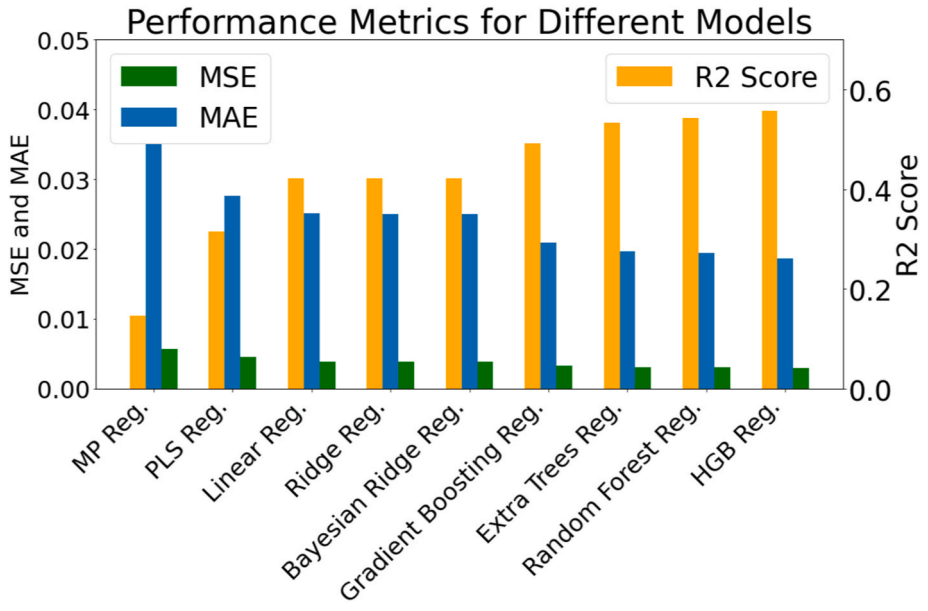

Fig. 8. Performance of 9 regression models to predict LAD based on QSM indexes.

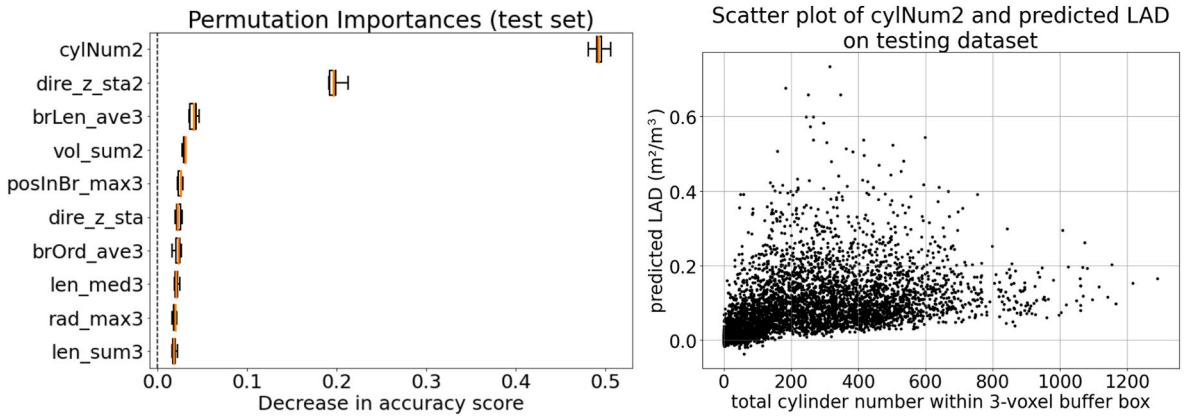

Fig. 9. Left: The 10 most important QSM indexes in LAD prediction using the Hist Gradient Boosting Regressor. The explanations for these index names are in Supplementary Table 2. Right: A scatter plot of the predicted LAD values in a testing dataset concerning the total cylinder numbers within a 3-voxel buffer box.

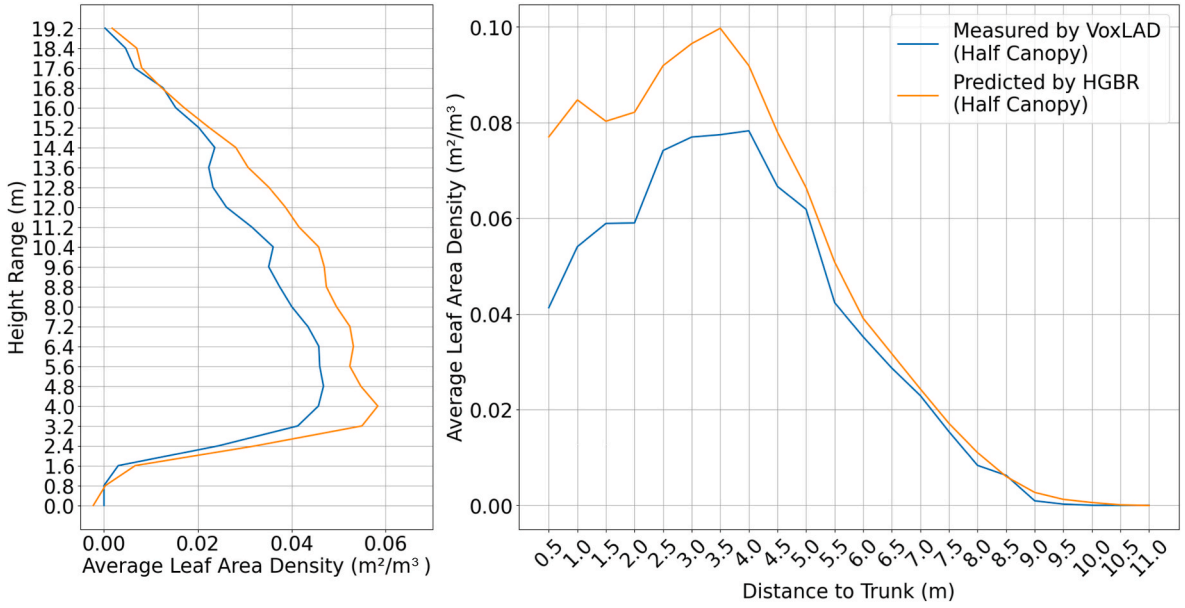

Fig. 10. Leaf Area and LAD distribution concerning the tree height and distance to the trunk.

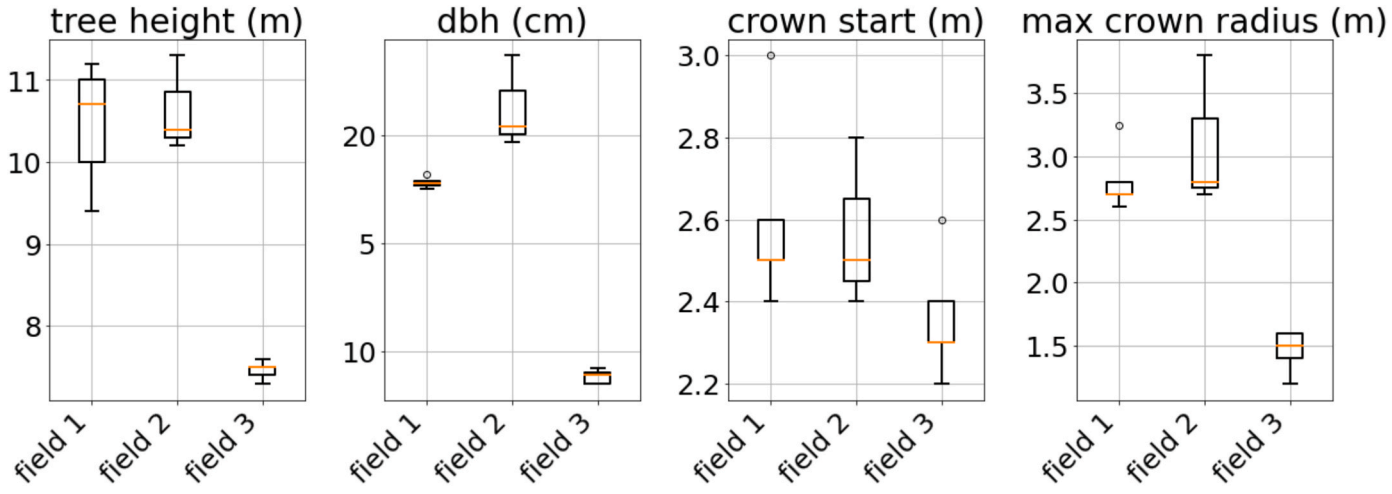

Fig. 11. Tree heights, DBH, crown start height, and crown radius of the 13 plane trees from the nursery. They were kept in three categories by their fields.

the LAD changes at different distances to the trunk is also well addressed in the predictions (see the orange line). However, from the center of the trunk until the peak of the LAD, the HGBR model always predicts roughly 20 % higher than the measured values.

3.3. Predictions on nursery trees in different sizes

To keep the clarity of different tree sizes, they were categorized by their fields (see Fig. 11): five trees from field 1 have a height of around 11 m and DBHs in ca. 18 cm; three trees from field 2 have a height of 10 m and DBHs of ca. 20 cm; five trees from field 3 have their heights of around 7.5 m and DBHs of ca. 9 cm. Their detailed measurements can be found in Supplementary Table 4.

To calculate the distributions of average leaf area per tree at different heights (see Fig. 12 left), the LAD values were multiplied by the volume of each voxel (0.512 m^3). For Munich Street trees, the validated voxels only came from the northeast side of the canopy facing the scanning positions. So, the leaf area shown with the red line in Fig. 12 left is only roughly half of the canopy.

In the LAD prediction of the 13 nursery trees, a similar distribution pattern to the Munich trees was also seen (see the blue, yellow, and green lines in Fig. 12). This indicated that the trained HGBR has learned the relation between LAD and branch distribution, instead of an absolute spatial location. In addition, their LAD distribution curves ran parallel through different heights. This was probably owing to the standardized maintenance in the nursery, causing their crown shapes to be scalable to different sizes. The crown shapes and branch densities of nursery trees differed from the street trees. So, the LAD curve had a different slope. This result showed the potential of this HGBR model in predicting the LAD of trees in an untrained crown shape and branch configuration.

An inaccuracy was noticed, where LAD outside the crowns was reduced slowly to 0.02 m^2/m^3 instead of approaching 0. This inaccurately indicated that the voxel length of 0.8 m or the sizes of the surrounding boxes did not suit those smaller trees with crown diameters of 3–6 m. At least, a sharp crown edge could not be acquired by this trained HGBR model.

Finally, the LAI values by summing up the LAD voxels by the HGBR model were compared with the ones by hemisphere images (see Fig. 13). Overall, the LAI by the HGBR model was smaller for younger trees in fields 3 and 1, whose DBH is much smaller than the Munich trees. This indicates again the limitation of adapting the prediction model to different tree crown sizes. However, the average LAI by HGBR in field 2, whose DBH was ca. 20 cm, achieved very close LAI values by the hemispherical photographs, barely 0.12 m^2/m^2 (9.57 %) higher.

4. Discussion

In a summary of the results above, the MAE and R2-score of the HGB Regression Model showed a good capability of this model from a statistical perspective. The predicted values were aligned with LAD ranges of urban trees in other studies (i.e., Alonzo et al. (2015); Hosoi et al. (2013); Soma et al. (2021)). The most effective variables among QSM indexes in our prediction model are the cylinder numbers and the average height difference of the cylinder starting to the voxel center within its 3-voxel buffer box. In our common sense, these factors are also closely related to the positions of the leaf growth.

In a closer look at the predicted LAD values, their distributions were also logical. As Fig. 10 shows, they followed precisely how the LAD changes concerning the tree height and distance to the trunk. The crown core center was the only crown area where the prediction became less precise. The branches were dense in this area, but the leaf density was low, even though the deviation was kept within 20 %.

Based on these analyses, we consider HGBR capable of predicting LAD in voxels based on the QSM. Nevertheless, the limitations and transferability of this model to other cases are discussed below.

4.1. Implementing VoxLAD to estimate voxel-based LAD from multiple scans

Using VoxLAD to estimate the LAD of trees, former studies mainly focused on only one tree sample and made at least 4 scans from all sides (Wei et al., 2020; D. Wu et al., 2018). To find statistical patterns between QSMs and predicted LAD, our study requires a larger number of trees in the TLS scan. We utilized an existing database (Yazdi et al., 2024) to balance the workload and added leaf-on scans on this base. One shortcoming of this dataset was the restrained access for LiDAR scanning from all sides of the street trees. Therefore, the limitations in VoxLAD using only one-sided scans along linear street trees are worth deeper analysis and validation in future studies.

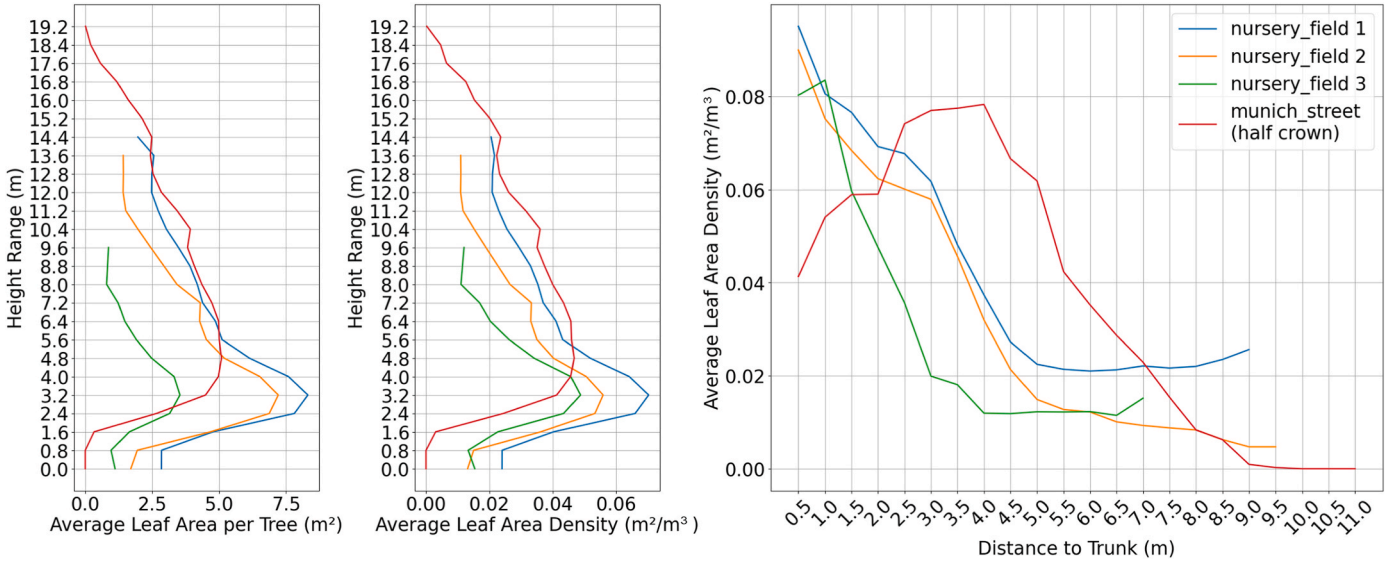

Fig. 12. Comparison between predicted LAD distributions on the younger trees at the nursery and street trees in Munich. Left: Average leaf area per tree in square meters at different heights. Middle: Average leaf area density per cubic meter at different heights. Right: Average leaf area density per cubic meter at different distances to the trunk.

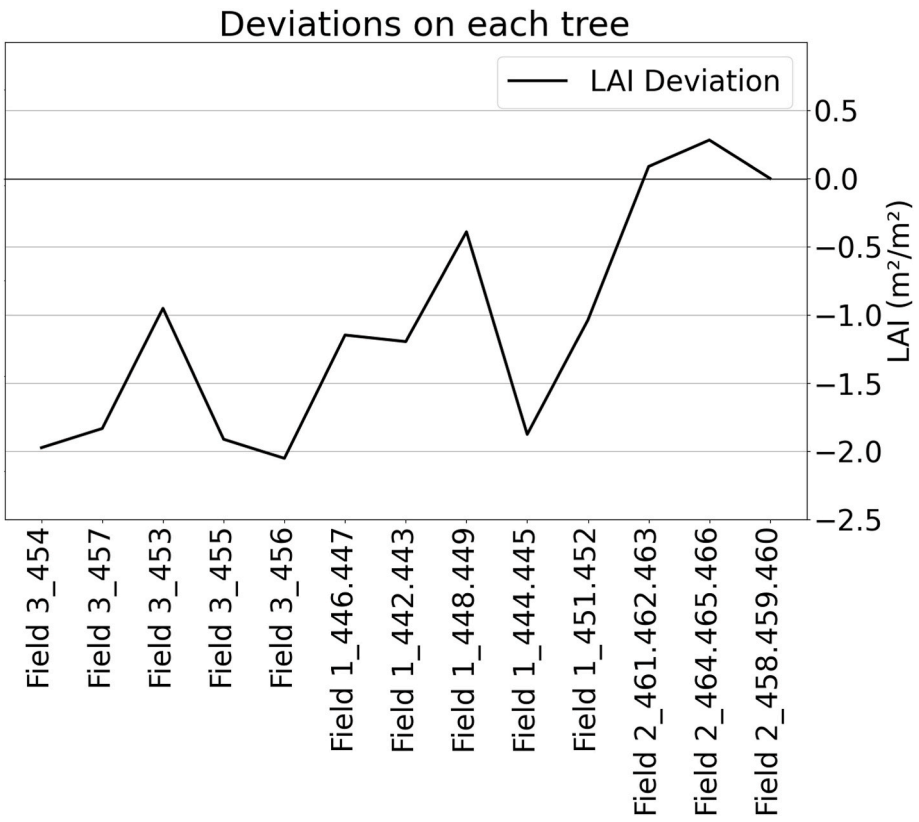

Fig. 13. Deviation of the average LAI calculations between the HGBR model and the hemisphere images. The trees were listed in ascending order according to their DBH from left to right.

4.2. Limited accuracy on twigs in QSMs

For reconstructing QSMs out of point clouds, the radius, consequently the volume of the most thin twigs and branches, can be overestimated up to over 50 % (Bornand et al., 2023; Demol et al., 2022). Such deviation is assumed to be higher at the upper part of the crowns than the lower crown because 1) their distances to the scanners were more considerable; 2) the thinner branches have a higher chance to swing in the wind. However, this difference in the deviation has not been calibrated. It can cause fewer clear differences in cylinder radius between young shoots and older branches. This may have prevented the regression models from gaining an even higher performance.

4.3. Impact of the voxel size and the buffer boxes on the performance

In both estimating the voxel-based LAD and abstracting the QSM index, the voxel size was the most crucial variable that could affect the precision and performance of this method. The voxel size tested in this study was only 0.8 m in each length. The tested buffer boxes were fixed to 3- and 5-times the voxel length. The size of the buffer boxes does not need to be an integer multiple of the voxel side length.

In the application to nursery trees (see section 3.3), it was noticed that this chosen scale was oversized for the younger trees with a crown radius of 1–3 m. The consequence was an inaccuracy at the edge of the crown, where the predicted LAD was not sharply reduced to zero. Smaller voxels would require much more computing resources and take more extensive storage, thus not being tested yet in this study.

The authors tested to train an HGBR model without the 5-voxel buffer box. However, the r-squared score was sharply reduced to 0.43. Although this buffer box of 4 m in length seemed oversized in a common first visual impression, it proved helpful in improving the prediction accuracy.

In addition, the complexity of this problem lies not only in adjusting the single voxel size but also in its relative size to the tree's crown, leaf shape, and leaf size, as well as the average distance between tree branches. These parameters would vary by species and their age. It was also challenging to explore combinations of a proper voxel size with a best-fitting buffer box to include the most effective cylinders in their surroundings. These were areas that required further experiments.

4.4. The overestimation at the crown center

This deviation and problems of less precise estimations in the crown center are common problems in estimating leaf area, LAD or LAI with all the other indirect methods, such as scanning with terrestrial or airborne scanners (Slavík et al., 2020; Viña et al., 2011; Xing et al., 2016), hemispherical imagery (Fuentes et al., 2008; Z. Liu et al., 2015), LAI2000 or LAI2200 (Behera et al., 2010; Poblete-Echeverría et al., 2015) or with a smartphone (Confalonieri et al., 2013). This difference is mainly related to clumping branches and leaves in the crown (Weiss et al., 2004) and the measurement of light transmission through the crown (Poblete-Echeverría et al., 2015).

Indeed, those branches at the crown center do not grow many leaves on them. We explored possibilities to bypass this problem by Eliminating cylinders with small branch orders. Cylinders with branch order 0 are the main stem. Cylinders with branch order 1 are primary branches, and so on. Specifically, we trained HGBR models using QSM indexes of cylinders with branch orders larger than 3, 5, and 7, respectively. In our experiments, removing cylinders until a higher branch order will reduce the r-squared score (see Supplementary Fig. 5). Although the predicted LAD peak at the crown center will be reduced (see Supplementary Fig. 6), these predictions do not necessarily shift more precisely to the reference values. So, our primary tests could not support eliminating low-branch-ordered cylinders to solve the overestimation problem.

4.5. About the calculated LAI values by hemispherical images

Admittedly, the most accurate way of understanding the index of leaves, such as LAD and LAI, is still to collect real leaves. However, this approach is not commonly conducted in forestry studies owing to its high labor demands, difficulties in practical implementation, and destructiveness (Alonzo et al., 2015; Chianucci et al., 2015). Therefore, digital photography has become popular for estimating LAI and leaf area in urban trees due to its simple, fast, and cost-effective procedures (Chianucci et al., 2015; Peper and McPherson, 1998). However, the analysis process is based on classifying pixels in the crown and sky, which highly depends on the light regime. In urban areas, structures like buildings are ignored and must be manually covered. Slight differences in cutting the edge of the crown could cause significant variance in the results. This could lead to a strong over- or underestimation of the resulting LAI values.

Despite limitations in LAI calculations by hemispherical photographs, Plane trees are known as sparsely foliated trees. They often don't have high LAI values. The predicted LAI values, mostly ranging between 1.2 and 2 m^2/m^2, were comparable with LAI for Plane trees measured by other researchers (Alonzo et al., 2015). Especially for individual trees in urban areas, these methods, typically applied in forestry, like the hemispherical imagery, were even criticized by Zhang et al. (2023). TLS methods, such as VoxLAD, used in this paper could be more likely to provide accurate data.

Still, all indirect methods, including our approach, should undergo a calibration process to reduce the error in the measurement approach. Although tedious and labor-intensive, direct measurements by leaf sampling and leaf area measurement (Zhang et al., 2023) can help to reduce the error in measuring leaf area and density.

5. Conclusion

Derived from the detailed TLS scans of trees, existing methods can extract geometrical and topological information from tree branches in the form of quantitative structure models (Raumonen et al., 2013) and leaf density distribution in the form of voxels (Béland et al., 2011). Together, they complete the critical data of a tree above the ground to analyze its function and growth (Shu et al., 2022). These data for deciduous trees must be collected separately during their leaf-on and leaf-off seasons, leading to a substantial workload and redundant data collection. Additionally, due to current technical limitations, TLS cannot capture every fine twig that connects to individual leaves in the leaf-off state and many other features (i.e. bark and nodes) are overlooked in QSMs. Inspired by the research using branch geometry described by the L-system to simulate the Leaf Area Density of virtual tree crowns (Jin and Tamura, 2012), this study aimed to explore the feasibility of using QSMs to predict the voxel-based LAD of real trees.

Leaf-on and leaf-off TLS of 16 *P. x hispanica* (around 20 m in height) standing on one street were used for this primary study. Their QSMs were extracted from leaf-off scans using treeQSM, while VoxLAD was applied to leaf-on scans to estimate their LADs. We novelly interpreted QSMs into QSM indexes to link these two data types, which associate cylinder distributions to voxels. The principle was to allocate cylinders to the voxels if they were directly contained in the voxel or if they were within a defined surrounding space. Then, the statistics of these cylinders, such as their length, radius, volume, relative positions to the voxel center, and so on, are composed of the QSM indexes. In this primary study, we set the voxel length to 0.8 m for a primary test. A close and far range of surrounding spaces was defined using boundary boxes of 3 and 5 times the voxel length, respectively. 12 standard regression models were tested to predict the LAD value for each voxel using its QSM indexes. Among them, the Hist Gradient Boosting Regressor performed the best. In this regression model, the total cylinder number and the average height differences from the voxel center to the cylinder start within this voxel's close-range surrounding space (2.4 m in length), contributing to more than 70 % predicting accuracy. Its R-squared score was 0.56, and the mean absolute error in the LAD prediction was 0.0187 m^2/m^3, being 16.33 % of the average LAD values in non-zero voxels. The major deviation only occurred at the center of the crown, where the branches were dense while the leaves were few.

With these results from our preliminary tests, this study has illustrated the potential of the novel QSM indexes in predicting voxel-based LAD using QSM. This trained model has been applied to plane trees of various sizes at a nursery. The predicted LAD was mapped on the ground to LAI maps. The average LAI for the trees with the largest DBH, the closet size of the street trees in Munich, has achieved a small difference of only 0.12 m^2/m^2 (9.57 %) to the LAI values measured by hemispherical photographs.

Further experiments will enhance our understanding regarding how far this model could adapt to trees with various sizes and crown shapes. Determining how the voxel size should adapt to different species with various crown shapes, branch densities, and leaf areas remains challenging.

CRediT authorship contribution statement

Qiguan Shu: Writing – review & editing, Writing – original draft, Visualization, Validation, Software, Project administration, Methodology, Investigation, Formal analysis, Data curation, Conceptualization. **Thomas Rötzer:** Writing – review & editing, Supervision, Resources, Investigation, Funding acquisition. **Hadi Yazdi:** Writing – review & editing, Methodology, Investigation. **Astrid Reischl:** Writing – review & editing, Writing – original draft, Software, Methodology. **Ferdinand Ludwig:** Writing – review & editing, Supervision, Resources, Project administration, Funding acquisition, Conceptualization.

Funding

This study is funded by the DFG-DACH project under No. DFG-GZ: LU2505/2-1 AOBJ:683826 427 and cooperated with other DFG funded research groups under PR 292/23-1, RO 4283/2-1 and No. 437788427-RTG2679.

Declaration of competing interest

The authors declare the following financial interests/personal relationships which may be considered as potential competing interests: Ferdinand Ludwig reports financial support was provided by German Research Foundation. Thomas Roetzer reports financial support was provided by German Research Foundation. If there are other authors, they declare that they have no known competing financial interests or personal relationships that could have appeared to influence the work reported in this paper.

Acknowledgment

Prof. Martin Beland shared his VoxLAD model in the newest version to enable this pioneering experiment. Bruns Pflanzen (Tree Nursery) provided access to plane trees of various sizes. Luke Bohnhorst coordinated the use of the RIEGL LiDAR scanner and the RISCAN Pro license in this study.

Appendix A. Supplementary data

Supplementary data to this article can be found online at https://doi.org/10.1016/j.srs.2025.100246.

Data availability

I have shared the link to my data at the attached file.

References

Abegg, M., Kükenbrink, D., Zell, J., Schaepman, M.E., Morsdorf, F., 2017. Terrestrial laser scanning for forest inventories—tree diameter distribution and scanner location impact on occlusion. Forests 8 (6). https://doi.org/10.3390/f8060184. Article 6.

Akay, A.E., Oğuz, H., Karas, I.R., Aruga, K., 2009. Using LiDAR technology in forestry activities. Environ. Monit. Assess. 151 (1), 117–125. https://doi.org/10.1007/s10661-008-0254-1.

Åkerblom, M., Kaitaniemi, P., 2021. Terrestrial laser scanning: a new standard of forest measuring and modelling? Ann. Bot. 128 (6), 653–662. https://doi.org/10.1093/aob/mcab111.

Alonzo, M., Bookhagen, B., McFadden, J.P., Sun, A., Roberts, D.A., 2015. Mapping urban forest leaf area index with airborne lidar using penetration metrics and allometry. Rem. Sens. Environ. 162, 141–153. https://doi.org/10.1016/j.rse.2015.02.025.

Alós Ortí, M., Casanelles-Abella, J., Chiron, F., Deguines, N., Hallikma, T., Jaksi, P., Kwiatkowska, P.K., Moretti, M., Muyshondt, B., Niinemets, Ü., Pinho, P., Pinto, M.J., Saar, P., Samson, R., Tryjanowski, P., Van Mensel, A., Laanisto, L., 2022. Negative relationship between woody species density and size of urban green spaces in seven European cities. Urban For. Urban Green. 74, 127650. https://doi.org/10.1016/j.ufug.2022.127650.

Armson, D., Stringer, P., Ennos, A.R., 2013. The effect of street trees and amenity grass on urban surface water runoff in Manchester, UK. Urban For. Urban Green. 12 (3), 282–286. https://doi.org/10.1016/j.ufug.2013.04.001.

Asef, S., Tolba, O., Fahmy, A., 2020. The effect of leaf area index and leaf area density on urban microclimate. J. Eng. Appl. Sci. 67, 427–446.

Behera, S.K., Srivastava, P., Pathre, U.V., Tuli, R., 2010. An indirect method of estimating leaf area index in *Jatropha curcas* L. using LAI-2000 Plant Canopy Analyzer. Agric. For. Meteorol. 150 (2), 307–311. https://doi.org/10.1016/j.agrformet.2009.11.009.

Béland, M., Widlowski, J.-L., Fournier, R.A., 2014. A model for deriving voxel-level tree leaf area density estimates from ground-based LiDAR. Environ. Model. Software 51, 184–189. https://doi.org/10.1016/j.envsoft.2013.09.034.

Béland, M., Widlowski, J.-L., Fournier, R.A., Côté, J.-F., Verstraete, M.M., 2011. Estimating leaf area distribution in savanna trees from terrestrial LiDAR measurements. Agric. For. Meteorol. 151 (9), 1252–1266. https://doi.org/10.1016/j.agrformet.2011.05.004.

Bolund, P., Hunhammar, S., 1999. Ecosystem services in urban areas. Ecol. Econ. 29 (2), 293–301. https://doi.org/10.1016/S0921-8009(99)00013-0.

Bornand, A., Rehush, N., Morsdorf, F., Thürig, E., Abegg, M., 2023. Individual tree volume estimation with terrestrial laser scanning: evaluating reconstructive and allometric approaches. Agric. For. Meteorol. 341, 109654. https://doi.org/10.1016/j.agrformet.2023.109654.

Calders, K., Adams, J., Armston, J., Bartholomeus, H., Bauwens, S., Bentley, L.P., Chave, J., Danson, F.M., Demol, M., Disney, M., Gaulton, R., Krishna Moorthy, S.M., Levick, S.R., Saarinen, N., Schaaf, C., Stovall, A., Terryn, L., Wilkes, P., Verbeeck, H., 2020. Terrestrial laser scanning in forest ecology: expanding the horizon. Rem. Sens. Environ. 251, 112102. https://doi.org/10.1016/j.rse.2020.112102.

Chianucci, F., Pisek, J., Raabe, K., Marchino, L., Ferrara, C., Corona, P., 2018. A dataset of leaf inclination angles for temperate and boreal broadleaf woody species. Ann. For. Sci. 75 (2), 50. https://doi.org/10.1007/s13595-018-0730-x.

Chianucci, F., Puletti, N., Giacomello, E., Cutini, A., Corona, P., 2015. Estimation of leaf area index in isolated trees with digital photography and its application to urban forestry. Urban For. Urban Green. 14 (2), 377–382. https://doi.org/10.1016/j.ufug.2015.04.001.

Confalonieri, R., Foi, M., Casa, R., Aquaro, S., Tona, E., Peterle, M., Boldini, A., De Carli, G., Ferrari, A., Finotto, G., Guarneri, T., Manzoni, V., Movedi, E., Nisoli, A., Paleari, L., Radici, I., Suardi, M., Veronesi, D., Bregaglio, S., et al., 2013. Development of an app for estimating leaf area index using a smartphone. Trueness and precision determination and comparison with other indirect methods. Comput. Electron. Agric. 96, 67–74. https://doi.org/10.1016/j.compag.2013.04.019.

Delagrange, S., Jauvin, C., Rochon, P., 2014. PypeTree: a tool for reconstructing tree perennial tissues from point clouds. Sensors (Peterb., NH) 14 (3). https://doi.org/10.3390/s140304271. Article 3.

Demol, M., Wilkes, P., Raumonen, P., Krishna Moorthy, S.M., Calders, K., Gielen, B., Verbeeck, H., 2022. Volumetric overestimation of small branches in 3D reconstructions of *Fraxinus excelsior*. Silva Fenn. 56 (1). https://www.silvafennica.fi/article/10550/selected/10550.

Dissegna, M.A., Yin, T., Wei, S., Richards, D., Grêt-Regamey, A., 2019. 3-D reconstruction of an urban landscape to assess the influence of vegetation in the radiative budget. Forests 10 (8). https://doi.org/10.3390/f10080700. Article 8.

Döllner, J., de Amicis, R., Burmeister, J.-M., Richter, R., 2023. Forests in the digital age: concepts and technologies for designing and deploying forest digital twins. Proceedings of the 28th International ACM Conference on 3D Web Technology, pp. 1–12. https://doi.org/10.1145/3611314.3616067.

Du, S., Lindenbergh, R., Ledoux, H., Stoter, J., Nan, L., 2019. AdTree: accurate, detailed, and automatic modelling of laser-scanned trees. Remote Sens. 11 (18). https://doi.org/10.3390/rs11182074. Article 18.

Duinker, P.N., Ordóñez, C., Steenberg, J.W.N., Miller, K.H., Toni, S.A., Nitoslawski, S.A., 2015. Trees in Canadian cities: indispensable life form for urban sustainability. Sustainability (Basel) 7 (6). https://doi.org/10.3390/su7067379. Article 6.

Eyster, H.N., Beckage, B., 2023. Arboreal urban cooling is driven by leaf area index, leaf boundary layer resistance, and dry leaf mass per leaf area: evidence from a system dynamics model. Atmosphere 14 (3). https://doi.org/10.3390/atmos14030552. Article 3.

Fan, G., Nan, L., Dong, Y., Su, X., Chen, F., 2020. AdQSM: a new method for estimating above-ground biomass from TLS point clouds. Remote Sens. 12 (18). https://doi.org/10.3390/rs12183089. Article 18.

Fuentes, S., Palmer, A.R., Taylor, D., Zeppel, M., Whitley, R., Eamus, D., 2008. An automated procedure for estimating the leaf area index (LAI) of woodland ecosystems using digital imagery, MATLAB programming and its application to an examination of the relationship between remotely sensed and field measurements of LAI. Funct. Plant Biol. 35 (10), 1070–1079. https://doi.org/10.1071/FP08045.

Girardeau-Montaut, D., 2023. Cloud-to-Cloud distance—CloudCompareWiki [Open-source document]. Cloud-to-Cloud Distance. https://www.cloudcompare.org/doc/wiki/index.php/Cloud-to-Cloud_Distance.

Grau, E., Durrieu, S., Fournier, R., Gastellu-Etchegorry, J.-P., Yin, T., 2017. Estimation of 3D vegetation density with Terrestrial Laser Scanning data using voxels. A sensitivity analysis of influencing parameters. Rem. Sens. Environ. 191, 373–388. https://doi.org/10.1016/j.rse.2017.01.032.

Hackenberg, J., Spiecker, H., Calders, K., Disney, M., Raumonen, P., 2015. SimpleTree—an efficient open source tool to build tree models from TLS clouds. Forests 6 (11). https://doi.org/10.3390/f6114245. Article 11.

Hemmerling, R., Kniemeyer, O., Lanwert, D., Kurth, W., Buck-Sorlin, G., 2008. The rule-based language XL and the modelling environment GroIMP illustrated with simulated tree competition. Funct. Plant Biol. 35 (10), 739–750. https://doi.org/10.1071/FP08052.

Hosoi, F., Nakai, Y., Omasa, K., 2013. Voxel tree modeling for estimating leaf area density and woody material volume using 3-D LIDAR data. In: *ISPRS Annals Of the Photogrammetry, Remote Sensing And Spatial Information Sciences, II-5-W2*, 115–120. WG V/3, I/2, I/3, III/2, V/2, VII/7, ICWG I/Va ISPRS Workshop Laser Scanning 2013 (Volume II-5/W2) - 11–13 November 2013, Antalya, Turkey. https://doi.org/10.5194/isprsannals-II-5-W2-115-2013.

Hu, R., Bournez, E., Cheng, S., Jiang, H., Nerry, F., Landes, T., Saudreau, M., Kastendeuch, P., Najjar, G., Colin, J., Yan, G., 2018. Estimating the leaf area of an individual tree in urban areas using terrestrial laser scanner and path length distribution model. ISPRS J. Photogrammetry Remote Sens. 144, 357–368. https://doi.org/10.1016/j.isprsjprs.2018.07.015.

Jiang, H., Hu, R., Yan, G., Cheng, S., Li, F., Qi, J., Li, L., Xie, D., Mu, X., 2021. Influencing factors in estimation of leaf angle distribution of an individual tree from terrestrial laser scanning data. Remote Sens. 13 (6). https://doi.org/10.3390/rs13061159. Article 6.

Jin, S., Tamura, M., 2012. Isolated tree 3D modeling: based on photographing leaf area density(LAD) calculation and L-system method. Land Surf. Rem. Sens. 8524, 135–142. https://doi.org/10.1117/12.977273.

Jonckheere, I., Nackaerts, K., Muys, B., van Aardt, J., Coppin, P., 2006. A fractal dimension-based modelling approach for studying the effect of leaf distribution on LAI retrieval in forest canopies. Ecol. Model. 197 (1), 179–195. https://doi.org/10.1016/j.ecolmodel.2006.02.036.

Kim, A., Olsen, R., Beland, M., 2015. Simulation of small footprint full waveform LIDAR propagation through a tree canopy in 3D. Proc. SPIE Int. Soc. Opt. Eng. 9465. https://doi.org/10.1117/12.2177158.

Kowarik, I., Fischer, L.K., Kendal, D., 2020. Biodiversity conservation and sustainable urban development. Sustainability (Basel) 12 (12). https://doi.org/10.3390/su12124964. Article 12.

Krisanski, S., Taskhiri, M.S., Gonzalez Aracil, S., Herries, D., Turner, P., 2021. Sensor agnostic semantic segmentation of structurally diverse and complex forest point clouds using deep learning. Remote Sens. 13 (8). https://doi.org/10.3390/rs13081413. Article 8.

Krishna Moorthy, S.M., Calders, K., Vicari, M.B., Verbeeck, H., 2020. Improved supervised learning-based approach for leaf and wood classification from LiDAR point clouds of forests. IEEE Trans. Geosci. Rem. Sens. 58 (5), 3057–3070. https://doi.org/10.1109/TGRS.2019.2947198.

Krishnamurthy, K.V., Bahadur, B., John Adams, S., Venkatasubramanian, P., 2015. Origin, development and differentiation of leaves. In: Bahadur, B., Venkat Rajam, M., Sahijram, L., Krishnamurthy, K.V. (Eds.), Plant Biology and Biotechnology: Volume I: Plant Diversity, Organization, Function and Improvement. Springer, India, pp. 153–175. https://doi.org/10.1007/978-81-322-2286-6_5.

Kroeger, T., McDonald, R.I., Boucher, T., Zhang, P., Wang, L., 2018. Where the people are: current trends and future potential targeted investments in urban trees for PM10 and temperature mitigation in 27 U.S. Cities. Landsc. Urban Plann. 177, 227–240. https://doi.org/10.1016/j.landurbplan.2018.05.014.

Kükenbrink, D., Marty, M., Bösch, R., Ginzler, C., 2022. Benchmarking laser scanning and terrestrial photogrammetry to extract forest inventory parameters in a complex temperate forest. Int. J. Appl. Earth Obs. Geoinf. 113, 102999. https://doi.org/10.1016/j.jag.2022.102999.

Liu, J., Skidmore, A.K., Wang, T., Zhu, X., Premier, J., Heurich, M., Beudert, B., Jones, S., 2019. Variation of leaf angle distribution quantified by terrestrial LiDAR in natural European beech forest. ISPRS J. Photogrammetry Remote Sens. 148, 208–220. https://doi.org/10.1016/j.isprsjprs.2019.01.005.

Liu, Z., Wang, C., Chen, J.M., Wang, X., Jin, G., 2015. Empirical models for tracing seasonal changes in leaf area index in deciduous broadleaf forests by digital hemispherical photography. For. Ecol. Manag. 351, 67–77. https://doi.org/10.1016/j.foreco.2015.05.005.

Ludwig, F., Hensel, M., Rötzer, T., Ahmeti, A., Chen, X., Erdal, H.I., Reischel, A., Shu, Q., Tyc, J.M., Yazdi, H., 2024. Computational framework for novel urban green system design: conceptual basics and methods. JoDLA – J. Digit. Landsc. Architect. 2024.

Mcdonald, R., Colbert, M., Hamann, M., Simkin, R., Walsh, B., Ascensão, F., Barton, M., Crossman, K., Edgecomb, M., Elmqvist, T., Gonzalez, A., Güneralp, B., Haase, D., Hillel, O., Huang, K., Maddox, D., Mansur, A., Paque, J., Pereira, H., Sharp, R., 2018. Nature in the Urban Century: A Global Assessment of where and How to Conserve Nature for Biodiversity and Human Wellbeing.

Mkaouar, A., Kallel, A., Guidara, R., Rabah, Z.B., Sahli, T., Qi, J., Gastellu-Etchegorry, J.-P., 2019. Estimation of foliage structure properties using TLS data. IGARSS 2019 -

2019 IEEE Int. Geosci. Rem Sens. Symp. 6079–6082. https://doi.org/10.1109/IGARSS.2019.8900638.
Mkaouar, A., Kallel, A., Rabah, Z.B., Chahed, T.S., 2021. Joint estimation of leaf area density and leaf angle distribution using TLS point cloud for forest stands. IEEE J. Sel. Top. Appl. Earth Obs. Rem. Sens. 14, 11095–11115. https://doi.org/10.1109/JSTARS.2021.3120521. IEEE Journal of Selected Topics in Applied Earth Observations and Remote Sensing.
Park, J.-I., Park, J., Kim, K.-S., 2020. Fast and accurate desnowing algorithm for LiDAR point clouds. IEEE Access 8, 160202–160212. https://doi.org/10.1109/ACCESS.2020.3020266. IEEE Access.
Parsa, V.A., Salehi, E., Yavari, A.R., Bodegom, P. M. van, 2019. An improved method for assessing mismatches between supply and demand in urban regulating ecosystem services: a case study in Tabriz, Iran. PLoS One 14 (8), e0220750. https://doi.org/10.1371/journal.pone.0220750.
Pearcy, R.W., Muraoka, H., Valladares, F., 2005. Crown architecture in sun and shade environments: assessing function and trade-offs with a three-dimensional simulation model. New Phytol. 166 (3), 791–800. https://doi.org/10.1111/j.1469-8137.2005.01328.x.
Pedregosa, F., Varoquaux, G., Gramfort, A., Michel, V., Thirion, B., Grisel, O., Blondel, M., Prettenhofer, P., Weiss, R., Dubourg, V., Vanderplas, J., Passos, A., Cournapeau, D., Brucher, M., Perrot, M., Duchesnay, É., 2011. Scikit-learn: machine learning in Python. J. Mach. Learn. Res. 12 (85), 2825–2830.
Peper, P.J., McPherson, E.G., 1998. Comparison of five methods for estimating leaf area index of open-grown deciduous trees. Arboric. Urban For. 24 (2), 98–111. https://doi.org/10.48044/jauf.1998.013.
Poblete-Echeverría, C., Fuentes, S., Ortega-Farias, S., Gonzalez-Talice, J., Yuri, J.A., 2015. Digital cover photography for estimating leaf area index (LAI) in apple trees using a variable light extinction coefficient. Sensors (Peterb., NH) 15 (2). https://doi.org/10.3390/s150202860. Article 2.
Prusinkiewicz, P., Lindenmayer, A., 1996. The Algorithmic Beauty of Plants. Springer Science & Business Media.
Prusinkiewicz, P., Mündermann, L., Karwowski, R., Lane, B., 2001. The use of positional information in the modeling of plants. Proceedings of the 28th Annual Conference on Computer Graphics and Interactive Techniques, pp. 289–300. https://doi.org/10.1145/383259.383291.
Raabe, K., Pisek, J., Sonnentag, O., Annuk, K., 2015. Variations of leaf inclination angle distribution with height over the growing season and light exposure for eight broadleaf tree species. Agric. For. Meteorol. 214–215, 2–11. https://doi.org/10.1016/j.agrformet.2015.07.008.
Rahman, M.A., Franceschi, E., Pattnaik, N., Moser-Reischl, A., Hartmann, C., Paeth, H., Pretzsch, H., Rötzer, T., Pauleit, S., 2022. Spatial and temporal changes of outdoor thermal stress: influence of urban land cover types. Sci. Rep. 12 (1), 671. https://doi.org/10.1038/s41598-021-04669-8.
Rahman, M.A., Stratopoulos, L.M.F., Moser-Reischl, A., Zölch, T., Häberle, K.-H., Rötzer, T., Pretzsch, H., Pauleit, S., 2020. Traits of trees for cooling urban heat islands: a meta-analysis. Build. Environ. 170, 106606. https://doi.org/10.1016/j.buildenv.2019.106606.
Ralph, O.D., Jason, B.D., 2000. Lidar remote sensing for forestry. J. For. 98 (6), 44–46. https://doi.org/10.1093/jof/98.6.44.
Raumonen, P., 2022. TreeQSM/manual at master · InverseTampere/TreeQSM · GitHub. https://github.com/InverseTampere/TreeQSM/tree/master/Manual.
Raumonen, P., Kaasalainen, M., Åkerblom, M., Kaasalainen, S., Kaartinen, H., Vastaranta, M., Holopainen, M., Disney, M., Lewis, P., 2013. Fast automatic precision tree models from terrestrial laser scanner data. Remote Sens. 5 (2). https://doi.org/10.3390/rs5020491. Article 2.
Reid, W., Mooney, H., Cropper, A., Capistrano, D., Carpenter, S., Chopra, K., 2005. Millenn Ecosys. Asses. Ecosys. Human well-being: Synthesis. Island Press, Washington, DC, p. 39.
Riegl, L.M.S.G., 2009. RIEGL VZ-400 Laser Scanners. RIEGL Laser Measurement Systems GmbH, p. 8 (No. Latest News March 2009. http://www.riegl.com/uploads/tx_pxpriegldownloads/RIEGL_VZ-400_News_03-2009.pdf.
Rötzer, T., Rahman, M.A., Moser-Reischl, A., Pauleit, S., Pretzsch, H., 2019. Process based simulation of tree growth and ecosystem services of urban trees under present and future climate conditions. Sci. Total Environ. 676, 651–664. https://doi.org/10.1016/j.scitotenv.2019.04.235.
Rouzbeh Kargar, A., MacKenzie, R., Asner, G.P., van Aardt, J., 2019. A density-based approach for leaf area index assessment in a complex forest environment using a terrestrial laser scanner. Remote Sens. 11 (15). https://doi.org/10.3390/rs11151791. Article 15.
Sarlikioti, V., De Visser, P.H.B., Buck-Sorlin, G.H., Marcelis, L.F.M., 2011. How plant architecture affects light absorption and photosynthesis in tomato: towards an ideotype for plant architecture using a functional–structural plant model. Ann. Bot. 108 (6), 1065–1073. https://doi.org/10.1093/aob/mcr221.
Schneider, F.D., Kükenbrink, D., Schaepman, M.E., Schimel, D.S., Morsdorf, F., 2019. Quantifying 3D structure and occlusion in dense tropical and temperate forests using close-range LiDAR. Agric. For. Meteorol. 268, 249–257. https://doi.org/10.1016/j.agrformet.2019.01.033.
Shu, Q., Rötzer, T., Detter, A., Ludwig, F., 2022. Tree information modeling: a data exchange platform for tree design and management. Forests 13 (11). https://doi.org/10.3390/f13111955. Article 11.
Shu, Q., Yazdi, H., Rötzer, T., Ludwig, F., 2024. Predicting resprouting of Platanus × hispanica following branch pruning by means of machine learning. Front. Plant Sci. 15. https://doi.org/10.3389/fpls.2024.1297390.
Slavík, M., Kuželka, K., Modlinger, R., Tomášková, I., Surový, P., 2020. UAV laser scans allow detection of morphological changes in tree canopy. Remote Sens. 12 (22). https://doi.org/10.3390/rs12223829. Article 22.
Soma, M., Pimont, F., Dupuy, J.-L., 2021. Sensitivity of voxel-based estimations of leaf area density with terrestrial LiDAR to vegetation structure and sampling limitations: a simulation experiment. Rem. Sens. Environ. 257, 112354. https://doi.org/10.1016/j.rse.2021.112354.
Soma, M., Pimont, F., Durrieu, S., Dupuy, J.-L., 2018. Enhanced measurements of leaf area density with T-LiDAR: evaluating and calibrating the effects of vegetation heterogeneity and scanner properties. Remote Sens. 10 (10). https://doi.org/10.3390/rs10101580. Article 10.
Stovall, A.E.L., Masters, B., Fatoyinbo, L., Yang, X., 2021. TLSLeAF: automatic leaf angle estimates from single-scan terrestrial laser scanning. New Phytol. 232 (4), 1876–1892. https://doi.org/10.1111/nph.17548.
Strohbach, M.W., Haase, D., 2012. Above-ground carbon storage by urban trees in Leipzig, Germany: analysis of patterns in a European city. Landsc. Urban Plann. 104 (1), 95–104. https://doi.org/10.1016/j.landurbplan.2011.10.001.
Terryn, L., Calders, K., Åkerblom, M., Bartholomeus, H., Disney, M., Levick, S., Origo, N., Raumonen, P., Verbeeck, H., 2022. Analysing individual 3D tree structure using the R package ITSMe. Methods Ecol. Evol. 14. https://doi.org/10.1111/2041-210X.14026.
The MathWorks Inc, 2024. *MATLAB (R2023b)* (Version 23.2.0.2409890 (R2023b) Update 3). The MathWorks Inc [Win11]. https://www.mathworks.com.
Trochta, J., Krůček, M., Vrška, T., Král, K., 2017. 3D Forest: an application for descriptions of three-dimensional forest structures using terrestrial LiDAR. PLoS One 12 (5), e0176871. https://doi.org/10.1371/journal.pone.0176871.
Viña, A., Gitelson, A.A., Nguy-Robertson, A.L., Peng, Y., 2011. Comparison of different vegetation indices for the remote assessment of green leaf area index of crops. Rem. Sens. Environ. 115 (12), 3468–3478. https://doi.org/10.1016/j.rse.2011.08.010.
Wang, D., Brunner, J., Ma, Z., Lu, H., Hollaus, M., Pang, Y., Pfeifer, N., 2018. Separating tree photosynthetic and non-photosynthetic components from point cloud data using dynamic segment merging. Forests 9 (5). https://doi.org/10.3390/f9050252. Article 5.
Wei, S., Yin, T., Dissegna, M.A., Whittle, A.J., Ow, G.L.F., Yusof, M. L. Mohd, Lauret, N., Gastellu-Etchegorry, J.-P., 2020. An assessment study of three indirect methods for estimating leaf area density and leaf area index of individual trees. Agric. For. Meteorol. 292–293, 108101. https://doi.org/10.1016/j.agrformet.2020.108101.
Weiss, M., Baret, F., Smith, G.J., Jonckheere, I., Coppin, P., 2004. Review of methods for in situ leaf area index (LAI) determination: Part II. Estimation of LAI, errors and sampling. Agric. For. Meteorol. 121 (1), 37–53. https://doi.org/10.1016/j.agrformet.2003.08.001.
Weller, M., 2021. Tree inventory data of Central European cities – studies on the composition and structure of urban tree populations and derivation of ecosystem services. In: [Master Thesis, TU Munich]. School of Life Sciences.
Wilkes, P., Disney, M., Armston, J., Bartholomeus, H., Bentley, L., Brede, B., Burt, A., Calders, K., Chavana-Bryant, C., Clewley, D., Duncanson, L., Forbes, B., Krisanski, S., Malhi, Y., Moffat, D., Origo, N., Shenkin, A., Yang, W., 2023. TLS2trees: a scalable tree segmentation pipeline for TLS data. Methods Ecol. Evol. 14 (12), 3083–3099. https://doi.org/10.1111/2041-210X.14233.
Wit, C. T. de, 1965. Photosynthesis of Leaf Canopies, vol. 663. Pudoc. https://library.wur.nl/WebQuery/wurpubs/413358.
Wolf, K.L., Lam, S.T., McKeen, J.K., Richardson, G.R.A., van den Bosch, M., Bardekjian, A.C., 2020. Urban trees and human health: a scoping review. Int. J. Environ. Res. Publ. Health 17 (12). https://doi.org/10.3390/ijerph17124371. Article 12.
Wu, D., Phinn, S., Johansen, K., Robson, A., Muir, J., Searle, C., 2018. Estimating changes in leaf area, leaf area density, and vertical leaf area profile for mango, avocado, and macadamia tree crowns using terrestrial laser scanning. Remote Sens. 10 (11). https://doi.org/10.3390/rs10111750. Article 11.
Wu, Y., 2021. Application research of terrain mapping based on RIEGL 3D scanning system. IOP Conf. Ser. Earth Environ. Sci. 719 (4), 042058. https://doi.org/10.1088/1755-1315/719/4/042058.
Xing, Y.Q., Huo, D., You, H.T., Tian, X., Jiao, Y.T., Xie, J., Yao, S.T., 2016. Estimation of birch forest LAI based on single laser penetration index of airborne LiDAR data. Ying Yong Sheng Tai Xue Bao = J. Appl. Ecol. 27 (11), 3469–3478. https://doi.org/10.13287/j.1001-9332.201611.020.
Yazdi, H., Shu, Q., Ludwig, F., 2023. A target-driven tree planting and maintenance approach for next generation urban green infrastructure (UGI). JoDLA – J. Digit. Landsc. Architect. 8–2023, 178. https://doi.org/10.14627/537740019.
Yazdi, H., Shu, Q., Rötzer, T., Petzold, F., Ludwig, F., 2024. A multilayered urban tree dataset of point clouds, quantitative structure and graph models. Sci. Data 11 (1). https://doi.org/10.1038/s41597-023-02873-x. Article 1.
Yin, T., Cook, B.D., Morton, D.C., 2022. Three-dimensional estimation of deciduous forest canopy structure and leaf area using multi-directional, leaf-on and leaf-off airborne lidar data. Agric. For. Meteorol. 314, 108781. https://doi.org/10.1016/j.agrformet.2021.108781.
Zhang, H., Yao, R., Luo, Q., Yang, Y., 2023. Estimating the leaf area index of urban individual trees based on actual path length. Build. Environ. 245, 110811. https://doi.org/10.1016/j.buildenv.2023.110811.